Quantitative hard x-ray phase contrast imaging of micropipes in SiC

V. G. Kohn, T. S. Argunova, and J. H. Je

Citation: AIP Advances **3**, 122109 (2013); doi: 10.1063/1.4846236
View online: http://dx.doi.org/10.1063/1.4846236
View Table of Contents: http://aipadvances.aip.org/resource/1/AAIDBI/v3/i12
Published by the AIP Publishing LLC.

Quantitative hard x-ray phase contrast imaging of micropipes in SiC

V. G. Kohn,[1] T. S. Argunova,[2,a] and J. H. Je[3,b]
[1]*National Research Center "Kurchatov Institute", 123182, Moscow, Russia*
[2]*Ioffe Physical-Technical Institute, RAS, 194021 St. Petersburg, Russia*
[3]*X-ray Imaging Center, Department of Materials Science and Engineering, Pohang University of Science and Technology, San 31 Hyoja-dong, Namku, 790-784 Pohang, Republic of Korea*

(Received 18 August 2013; accepted 27 November 2013; published online 6 December 2013)

Peculiarities of quantitative hard x-ray phase contrast imaging of micropipes in SiC are discussed. The micropipe is assumed as a hollow cylinder with an elliptical cross section. The major and minor diameters can be restored using the least square fitting procedure by comparing the experimental data, i.e. the profile across the micropipe axis, with those calculated based on phase contrast theory. It is shown that one projection image gives an information which does not allow a complete determination of the elliptical cross section, if an orientation of micropipe is not known. Another problem is a weak accuracy in estimating the diameters, partly because of using pink synchrotron radiation, which is necessary because a monochromatic beam intensity is not sufficient to reveal the weak contrast from a very small object. The general problems of accuracy in estimating the two diameters using the least square procedure are discussed. Two experimental examples are considered to demonstrate small as well as modest accuracies in estimating the diameters. [http://dx.doi.org/10.1063/1.4846236]

I. INTRODUCTION

Micropipes are hollow tube-shaped defects which exist in diversity of crystalline materials. The formation of micropipes in silicon carbide (SiC) bulk crystals is associated with crystal lattice dislocations with large Burgers vectors. Their diameters range from a few ten nanometers to several ten micrometers.[1,2] Different from a number of techniques developed so far x-ray imaging based on phase contrast[3,4] or Bragg-diffraction[2,5,6] provides the only possibility to study them nondestructively. As far as the size concerns, a micropipe of 1 μm diameter is a very small object to visualize using x-ray phase contrast imaging, demanding a very high flux for an acceptable signal-to-noise ratio. A feasible way to observe such small micropipes at medium-brilliant third generation Synchrotron Radiation (SR) sources, like Pohang Light Source (PLS) in Korea, is to apply pink beam (see [7–10] and references therein).

The pink beam experimental setup is simple, and is shown in Fig. 1. X-ray beam from a SR source, controlled in its beam size by slits, illuminates an object such as a single crystal SiC plate containing micropipes. The transmitted x-ray beam is converted to visible light by a fluorescent crystal (scintillator) at some distance from the object. Then the visible image is magnified by optical lense system and finally captured by a CCD camera. The magnification allows one to reach a resolution up to fracture of microns.

As is known, phase contrast imaging technique demands coherent beam. In our experiment spatial (transverse) coherence is due to the very small source angular size at the object $\alpha = S/L$, at

[a]Also at Department of Materials Science and Engineering, Pohang University of Science and Technology
[b]Electronic mail: jhje@postech.ac.kr

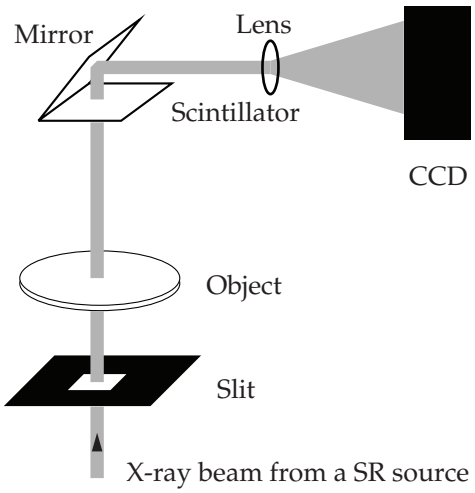

FIG. 1. A sketch of the experimental scheme for obtaining micropipe images. The SR beam, controlled in its beam size by a slit, illuminates the object. The transmitted beam illuminates a scintillator crystal which converts the x rays to a visible light. Then the image is magnified by a lens system and detected by CCD detector.

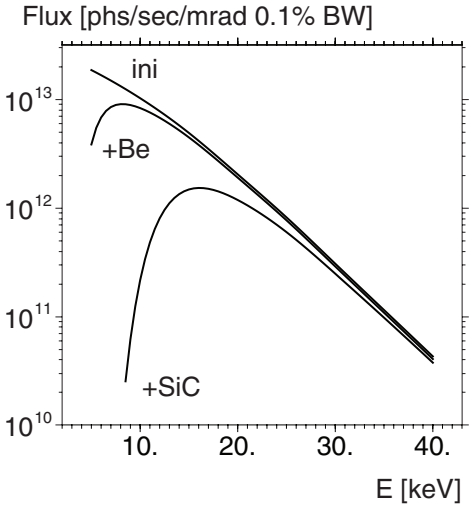

FIG. 2. A spectrum of the white SR beam at PLS. The upper curve is an initial spectrum. The middle curve is an effective spectrum after a passage of Be window. The lower curve is an effective spectrum behind the object – 490 μm thick SiC plate.

least, in the vertical plan. For example, the source size $S = 60$ μm for x-ray energy $E = 16$ keV (wave length $\lambda = 0.775$ Å) provides the transverse coherence length $L_{tc} = \lambda/\alpha = 42$ μm at the distance $L = 32$ m, which is much larger than typical diameter of micropipe cross section.

Meanwhile the temporal (longitudinal) coherence is related to the band width of the beam.[11] If the width of the radiation spectrum is effectively reducible to $\Delta\lambda$ somehow, then the longitudinal coherence length is estimated as $L_{lc} = \lambda^2/\Delta\lambda$. In our experiment we use the effective band width of SR pink beam which is formed as follows.

The SR intensity decreases as the energy increases. On the other hand, the x-ray absorption by the SiC crystal plate that contains micropipes leads to an interesting result: the intensity of the transmitted x-ray beam decreases as the energy decreases. As a result, the effective spectrum of pink beam SR in our case has a well pronounced peak, and an effective full width at half maximum (FWHM) $\Delta\lambda$. Figure 2 shows an effective spectrum, calculated for the PLS and a SiC crystal plate of thickness 490 μm, with a maximum at $\lambda = 0.775$ Å and FWHM $\Delta\lambda = 0.52$ Å. Applying the two

parameters, the temporal coherence is estimated as $L_{tc} = 1.2$ Å. Despite the very small value, it is sufficient to image the central part of micropipe.

Consider an example. Let a micropipe has a diameter $d = 2$ μm, and the object-to-detector (here, the scintillator) distance z_d is 30 cm. The optical path difference l between the central and the edge points at the detector is equal to $l = 0.5d(x + 0.25d)/z_d$ where x is the distance from the optical axis at the detector. For the central point of the image ($x = 0$) l is estimated as <0.02 Å. On the other hand, the equality $l = 1.2$ Å occurs at $x = 36$ μm.

However, to detect the interference between the rays inside and outside the micropipe, the size of the central (coherent) part of the image will be furthermore reduced. Nevertheless, our estimation shows that the interference can be seen in the central part of the image. We note that the image of such a small object is completely determined by interference in partially coherent radiation (pure phase contrast) because absorption is very small. As is known, coherence is not necessary for the images determined by absorption.

Next we try to obtain some quantitative information about the sizes of the elliptical cross section, i.e. the diameters across (D) and along (D_0) the beam from only one projection. Since the object, the SiC crystal plate, has a small thickness only in the direction normal to the surface (see Fig. 1), this direction must coincide with the beam direction to decrease an absorption.

Of course, this information can not be directly obtained from the image due to its interference nature, and theoretical simulations are necessary. The diameters can be determined by fitting the calculated profiles to the experimental ones. The article is devoted to discussion of some peculiarities of solution of such task. We elaborated the computer program FIMTIM (fit of microtube imaging) to simulate and fit the experimental data with the aim to determine the diameters D and D_0 of micropipe cross section.

The details of the computer program and fitting procedure are described in the next section. In section III we discuss the limits of information which can be obtained from only one projection image. These limits can not allow us to completely resolve the geometrical position of micropipe inside the crystal. Such information must be obtained independently. In section IV we discuss a question of estimating the accuracy of parameters from the least square fitting procedure. Finally, in section V we consider two experimental examples of applying the technique.

II. GENERAL SCHEME OF SIMULATING PHASE CONTRAST IMAGES OF MICROPIPES

The theory of x-ray phase contrast imaging is well known from the pioneer work by Snigirev *et al.*[12] We start from a monochromatic point source which radiates a spherical wave. We assume that our object, a micropipe, is homogeneous in one direction perpendicular to the beam direction (optical axis). In general case, the micropipe axis is not a straight line. However, it is sufficient to assume some part of the axis to be a straight line, if the length of this part exceeds the diameter of the first Fresnel zone $2(\lambda z_d)^{1/2}$. Here z_d is the distance from the object to the x-ray detector (scintillator). Then the wave function (the electric field) of the radiation in front of the object can be written as the Kirchhoff propagator

$$P(x, z_0) = \frac{1}{(i\lambda z_0)^{1/2}} \exp\left(i\pi \frac{x^2}{\lambda z_0}\right). \quad (1)$$

Here z_0 is the source-to-object distance along the beam (optical axis), and x is a coordinate across the beam. The homogeneous part of SiC crystal does not influence the image and can be neglected. We select a part of the crystal containing the micropipe as a hollow cylinder. In general case, the intersection region between the beam and the micropipe is elliptical.

A radiation transmission through the object is accounted for in the geometrical optics approximation where it is sufficient to calculate only the complex phase shift (including absorption) along the rays. Since our object is very small we can assume that all rays go parallel to the optical axis. As a result, we obtain the expression for the transmission function $T(x)$ as follows: if $|x| > R$ then $T(x)$

$= 1$, otherwise

$$T(x) = \exp\left([i\Phi + M] \left(1 - \frac{x^2}{R^2} \right)^{1/2} \right), \tag{2}$$

where

$$\Phi = \frac{4\pi}{\lambda} \delta R_0, \quad M = \Phi \frac{\beta}{\delta} \tag{3}$$

Here $R = D/2$, $R_0 = D_0/2$ are half diameters of the intersection elliptical cross section across and along the beam correspondingly, and $\delta - i\beta = 1 - n$, where n is the complex refractive index of the SiC. The wave function of the radiation behind the object is equal to $w_o(x) = T(x)P(x, z_0)$.

Transmission of the wave function through the air from the object to the detector is calculated by a convolution with the Kirchhoff propagator

$$w_d(x) = \int dx' P(x - x', z_d) T(x') P(x', z_0) \tag{4}$$

We are interested in the radiation relative intensity

$$I(x) = \frac{|w_d(x)|^2}{|P(x, z_t)|^2}. \tag{5}$$

For this value we can use properties of the Kirchhoff propagator and transform the result as follows

$$I(x) = |a(x_0)|^2, \quad a(x_0) = \int dx' P(x_0 - x', z_r) T(x') \tag{6}$$

where

$$x_0 = x \frac{z_0}{z_t}, \quad z_t = z_0 + z_d, \quad z_r = \frac{z_0 z_d}{z_t} \tag{7}$$

The integral has to be calculated in the infinite limits. It is convenient to transform the calculation procedure for $a(x)$ as a finite limits integral, as follows

$$a(x) = 1 + \int dx' P(x - x', z_r)[T(x') - 1] \tag{8}$$

Now the integrand is equal to zero outside the object, and we obtain effectively finite limits.

The intensity profile for the monochromatic point source does not match the experimental profile. Taking into account that various points on the source and various values of radiation energy are incoherent, it is sufficient to perform a convolution of the intensity profile with the Gaussian which represents the brightness of the source at the detector position, i.e. the source projection. The FWHM of such Gaussian is equal to $S_d = S z_d/z_0$. At the next step we calculate the set of image profiles for various x-ray energies and perform a summation over the radiation spectrum. The summation over the spectrum is performed on the set of energy points from 5 to 40 keV with a 1 keV step. The possibility to make a calculation with the twice smaller step has been elaborated as well.

III. THE CROSS-SECTION DIAMETERS AND THE REAL MICROPIPE DIAMETERS

As it follows from the preceding section, we consider two parameters, the two diameters of the intersection region of the micropipe by the x-ray beam: D across the beam (along x axis) and D_0 along the beam (along z axis). These values may not be equal to the real diameters of the micropipe cross section in the plane normal to the micropipe axis. In general case the micropipe axis makes the angle θ with the beam direction (z-axis).

Consider the case where the micropipe axis is parallel to the y axis, i.e. normal to the beam direction (z) as well as the image axis (x) and $\theta = 90^\circ$. Let us suppose that the micropipe has proper elliptical cross section with its major d and minor d_0 diameters, and the angle φ exists between the d-axis and the x-axis. The situation is illustrated in Fig. 3, where $\varphi = 45^\circ$.

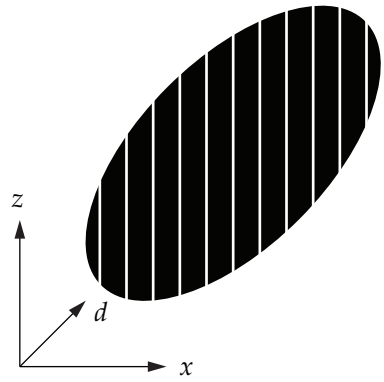

FIG. 3. A diagram showing a passage of x rays through a proper elliptical cross section of a micropipe. The cross section is shown by black elliptical area. White strips show the x-ray beam directions which are parallel to the z axes. The x axis is a direction which is normal to both the beam and the micropipe axis. This is the axis along which the intensity distribution is registered. The direction d coincides with the main axis of proper elliptical cross section. The angle between the d axis and the x axis $\varphi = 45^\circ$.

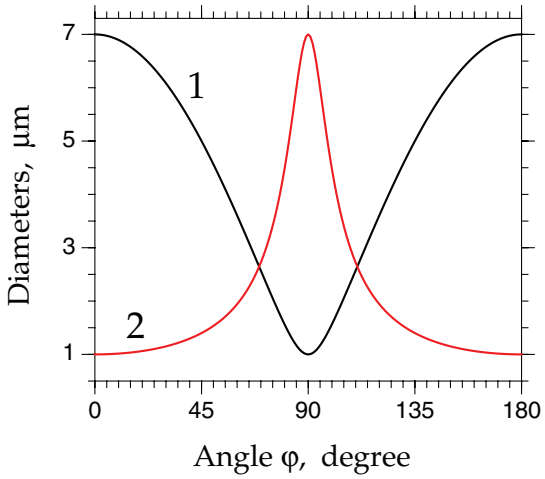

FIG. 4. The effective diameters of the micropipe cross section D (curve 1) and D_0 (curve 2) as functions of the rotating angle φ of a proper elliptical cross section.

We calculate the parameters D and D_0 of the transmission function (2) in terms of d and d_0 as follows

$$D = [(d\cos\varphi)^2 + (d_0\sin\varphi)^2]^{1/2}, \quad D_0 = d_0 d/D. \tag{9}$$

One can see that for the same elliptical cross-section of the micropipe, different values for D and D_0 can be obtained depending on the angle φ. However, one can not determine the angle value from only one projection. In principle, knowing this value one could solve the inverse problem of calculating d and d_0 from D and D_0. It is easy to see that the size of cross-section area is independent of φ.

Figure 4 shows two curves $D(\varphi)$ (black line) and $D_0(\varphi)$ (red line) for a particular case where $d = 7$ μm and $d_0 = 1$ μm. It is of interest that even for a strongly asymmetric elliptical cross section of micropipe we can obtain $D = D_0$ for the specific value of φ. The right side of the central part of this figure ($\varphi > 90^\circ$) is qualitatively similar to the result of fitting the parameters D and D_0 from experimental profiles taken at different points along the micropipe axis (see Fig. 6 in the article by

Argunova *et al.*[13]). We now can assume that the studied micropipe has the elliptical cross section which changes its orientation relative to the beam direction.

Let us consider another case where the micropipe has proper circular cross-section with a diameter d, but its axis makes the angle $\theta < 90^\circ$ with the beam direction (z axis). Such a situation arises if the micropipe axis is not parallel to the sample surface which is fixed normal to the beam direction in order to reduce the absorption. The case, considering above, where the micropipe axis is parallel to the crystal surface may exist sometimes, but it is not a general case. The experiment shows that there are many micropipes with the axes which approximately normal to the crystal plate surface. Therefore such micropipes make a small value of the angle θ, i.e. they approximately parallel to the beam direction.

It is assumed by Kohn *et al.*[14] that just such micropipes create unusual images, so called black contrast, where the central part of the image is black whereas normal images have white central part, see, for example, Fig. 1 in the paper by Kohn *et al.*.[7] In this case the parameters of the transmission function are $D = d$, $D_0 = d/\sin\theta$, $D_0 \gg D$. In principle, one can find two parameters d and θ from D and D_0, if to know exactly that the micropipe has proper circular cross section.

Even if the proper cross-section is circular with the diameter d, and $\theta = 90^\circ$ there is another possibility to find a micropipe with the axis which makes an angle $\psi < 90^\circ$ with the vertical plan (x, z), i.e. with the axis x inside the plan (x, y). In this case we have the next values $D = d/\sin\psi$, $D_0 = d$, $D > D_0$. This situation looks more simple because we can rotate the sample as a whole until the micropipe axis lies in a horizontal position. However, one 2D image of the sample as a whole may contain many images of micropipes, and some of them may be in a horizontal position, but the others may have the angle ψ. Even in this case we can rotate 2D image for the purpose of moving the specific micropipe axis in a horizontal position.

However, such a rotation will lead to a more complicated situation with the source size because in experiment the vertical source size only is small but the horisontal source size is much larger. In reality, all considered situations may occur simultaneously, impeding the determination of the proper micropipe diameters d and d_0 from the diameters D and D_0 of the intersection area. In this article we discuss only how to reconstruct the parameters D and D_0 by means of the fitting procedure when the experimental profile is compared with the theoretical profiles calculated according to the procedure described in the preceding section. To make the next step an additional information is necessary.

IV. LEAST-SQUARE FITTING AND ESTIMATION OF ACCURACY

The theoretical profile $I(x, D, D_0)$ is normalized in such a way that the tails far from the object are equal to unity, but the experimental profile $y_i = ex(x_i)$ is not normalized. Of course, we can calculate a mean value and divide the data on it. In principle, the mean value has to correspond to the tail value, but only in the infinite limits. However, we know only a finite number of points in the finite region. In addition, there is random noise in the data. That is why it is more convenient to introduce an additional parameter K whose value is calculated from a least-square fitting procedure, i.e. from the minimum

$$\chi^2 = \sum_{i=1}^{n} [I(x_i, D, D_0) - K y_i]^2 \tag{10}$$

It is easy to verify that

$$K = \frac{\langle I\, y\rangle}{\langle y^2\rangle}, \quad \langle o\rangle = \sum_{i=1}^{n} o_i \tag{11}$$

The formula (11) has to be applied for any values of D and D_0 if the minimum χ^2 value is searched by probing various values of D and D_0. When the minimum is reached, the K value has to be fixed. The next step is to estimate a reasonable accuracy of the found values. That is especially important in the case of micropipe. Indeed, it was shown by Kohn *et al.*[10] that for the micropipes with small values D and D_0 the theoretical profile strongly depends on the product DD_0 alone, i.e. on the cross-section area. This means that both values cannot be found with a significant accuracy.

Taking into account this point let us consider in detail the problem of accuracy in the least square fitting procedure. For simplicity we will assume that the points x_i are known explicitly, and only y_i are random values with the probability

$$W(y_i) = \frac{1}{(2\pi)^{1/2}\sigma} \exp\left(-\frac{(y_i - I(x_i))^2}{2\sigma^2}\right) \tag{12}$$

where σ is dispersion. Since each experimental point is independent of other points, the total probability can be written as

$$L(y_1, \ldots y_n) = \left(\frac{1}{(2\pi)^{1/2}\sigma}\right)^n \exp\left(-\frac{1}{2\sigma^2}\chi^2\right) \tag{13}$$

Here we assume that all points have the same dispersion, and χ^2 is determined by eqs. (10) and (11).

It is easy to understand that the probability maximum is correspondent to the χ^2 minimum. Let us find the χ^2 minimum as a function of D and D_0. We denote it as $\chi^2_{\min}$. Then we can find σ from the condition of probability maximum as

$$\sigma^2 = \frac{\chi^2_{\min}}{n} \tag{14}$$

At this point we need to consider the problem from another side. We know the parameter D_m and D_{0m} for which $\chi^2 = \chi^2_{\min}$. Then we fix the coefficient K at this point, and consider the expression (13) as the probability for the parameters D and D_0. For small deviations $u_1 = D - D_m$ and $u_2 = D_0 - D_{0m}$ we have

$$\chi^2(u_1, u_2) = \chi^2_{\min} + \frac{1}{2}\sum_{i,k=1}^{2} A_{ik} u_i u_k \tag{15}$$

where

$$A_{ik} = \frac{\partial^2 \chi^2}{\partial u_i \partial u_k}\Big]_{u_1 = u_2 = 0} \tag{16}$$

If the term $A_{12} \neq 0$ then we cannot obtain an independent estimation of accuracy for various parameters. We need to introduce new parameters

$$v_i = \sum_{k=1}^{2} s_{ik} u_k \tag{17}$$

as linear combination of old parameters with the transformation matrix s_{ik} so that the matrix $g = s^{-1}As$ has diagonal form $g_i\delta_{ik}$. In the case of two parameters this task has analytical solution

$$s_{ik} = \begin{pmatrix} \cos\alpha & \sin\alpha \\ -\sin\alpha & \cos\alpha \end{pmatrix}, \quad \tan 2\alpha = \frac{2A_{12}}{A_{22} - A_{11}} \tag{18}$$

Then

$$2g_{1,2} = A_{11} + A_{22} \pm z\left[(A_{22} - A_{11})^2 + 2A_{12}^2\right]^{1/2} \tag{19}$$

where $z = -1$ if $A_{22} < A_{11}$, and $z = 1$ otherwise.

Finally we obtain

$$L(y_1, \ldots y_n) = \left(\frac{1}{2\pi\sigma^2 e}\right)^{n/2} \Pi_{i=1}^2 \exp\left(-\frac{g_i v_i^2}{4\sigma^2}\right) \tag{20}$$

Here $e = \exp(1)$. It is important here that the probability expression looks like a product of two Gaussians (not normalized) as functions of v_i. We can determine the error err_i of the parameter v_i

as FWHM of the Gaussian. Taking into account eq. (14) we have

$$err_i = 2.355 \left(\frac{2\chi^2}{ng_i} \right)^{1/2}_{\min} \tag{21}$$

This expression has a right dimension. It is of interest that it depends on $\chi^2_{\min}$. This looks to be right because the case $\chi^2_{\min} = 0$ is correspondent to exact comparison between the theoretical and experimental values. Another interesting point is a dependence on the number of experimental points n. A dependence on the second derivative is evident. As a result, we obtain in this approach three parameters: the angle α between the axes of deviations u_i and v_i and two accuracy parameters err_i. It may be described as follows: The curve $\chi^2 - \chi^2_{\min} = C$ has a form of ellipse whose axes make an angle α with the axes of the deviations u_i.

For example, if the theoretical curve depends only on the product DD_0 we can find that $\alpha = 45^\circ$, $v_1 \propto u_1 + u_2$ has definite accuracy, but $v_2 \propto u_2 - u_1$ is not defined. It is the reason why it is very important to examine the curves $\chi^2 - \chi^2_{\min} = C$ with various values of C. New version of our program FIMTIM can draw two-dimensional map of $\chi^2 - \chi^2_{\min}$ as a function of D and D_0 near the minimum point.

V. EXPERIMENTAL EXAMPLES

Phase contrast experiments have been performed at the third generation SR source in PLS, Korea operating at 2.5 GeV. At the 6D (X-ray micro-imaging) beamline the beam was extracted from a bending magnet port located at a distance of 32 m from a sample. The source size was 60 μm (vertically) and 160 μm (horizontally). The experimental setup is shown in Fig. 1, and the effective spectrum of the SR source is shown in Fig. 1. The detector was 14 bit CCD camera with 9 μm (H) x 9 μm (V) pixel size sensitive to a visible light. X rays were converted into visible light by a $CdWO_4$ crystal-scintillator 150 μm thick. The image was enlarged by an optical lens system. We used 20× lens which provided 0.45 μm x 0.45 μm effective pixel size. The CCD matrix of 4008×2672 pixels allowed us to have a view field of 1804×1202 μm size. Exposure times were chosen to obtain 12000 - 16000 count rates.

One 2D image (field of view) might contain several images of micropipes in different positions, and of various kinds. We chose the most horizontal micropipe, i.e. with the axis approximately along the y axis. Then we slightly rotated the image by means of the computer program ImageJ, if necessary, to place the micropipe axis strictly horizontal. After that we rotated the image on the 90° and the intensity profiles across the micropipe axis were registered numerically with ImageJ as one vertical level (horizontal line on the image). Sometimes two or more vertical levels were summed to increase the signal-to-noise ratio. Such an intensity profile as a function of one coordinate x was used for fitting with the above procedure. In this section we consider two different cases where the diameters D and D_0 have been determined with lower and higher accuracy.

Figure 5 shows the experimental data (markers) and the calculated intensity profile (solid line) for the values of $D = 1.44$ μm and $D_0 = 1.68$ μm which correspond to a minimum $\chi^2 = 1.08 \cdot 10^{-4}$ in the first case. The experimental data have the count rate of 12900 at the maximum. The experimental curve was normalized by means of the best coincidence with the theoretical curve as described above. The object-to-detector distance z_d was 35 cm. The important question for us is a level of accuracy of the obtained values. Figure 6 allows us to demonstrate a situation. It shows a dependence $\chi^2(D, D_0)$ near the minimum point as a linear black-white contrast with black color for $\chi^2 = 1.08 \cdot 10^{-4}$ and white color for $\chi^2 = 1.41 \cdot 10^{-4}$ or larger. One can see that the area of small χ^2 values is not localized. It has short dimension along the direction $D = D_0$ and long dimension along the normal direction.

Such a situation was described for the first time by Kohn *et al.*[10] It is caused by the fact that, for small values of micropipe diameters, the theoretical profile depends strongly on the product DD_0 alone. Moreover, only the maximum value depends on DD_0, while the profile itself has a universal form. There are several conditions for fulfilling such a situation: namely, the diameter D must be smaller than the first Fresnel zone diameter $2(\lambda z_d)^{1/2}$, and the phase shift $\Phi = (2\pi/\lambda)\delta D_0$ must be

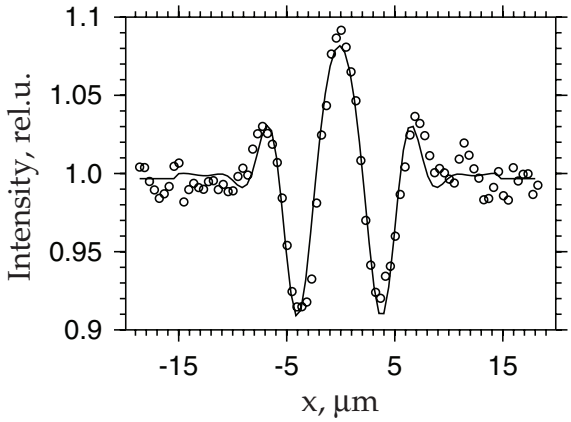

FIG. 5. Experimental data and simulated theoretical profile in the case of best coincidence for the first case. By fitting many profiles for various diameters of micropipe cross section we determined the diameters from the condition of best coincidence.

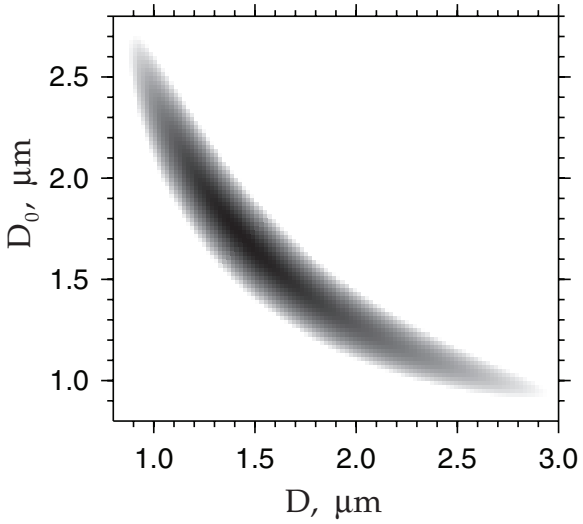

FIG. 6. A map showing the least square sum χ^2 as a function of D and D_0 in the first case. See text for details.

less than unity. Our case just meets these conditions. We obtain the following estimations of the parameters accuracy from (18) and (21): $\alpha = 40^\circ$, $err_1 = 0.09\ \mu$m and $err_2 = 0.73\ \mu$m.

As the second example, we consider the micropipe with diameters which don't meet the above conditions. The experimental data (markers) and the calculated intensity profile (solid line) are shown in Fig. 7 for values $D = 10.25\ \mu$m and $D_0 = 2.54\ \mu$m. The object-to-detector distance z_d was equal to 15 cm. In this case the coincidence is not pretty good because a minimum $\chi^2 = 4.01 \cdot 10^{-4}$. The maximum count rate was 14900. Figure 8 shows a dependence $\chi^2(D, D_0)$ near the minimum point in the same manner as Fig. 6, i.e.with black color used for $\chi^2 = 4.01 \cdot 10^{-4}$ and white color used for $\chi^2 = 5.21 \cdot 10^{-4}$ or larger. One can see that the area of small χ^2 is better localized. The estimations of the parameters accuracy from (18) and (21) are: $\alpha = -6^\circ$, $err_1 = 0.12\ \mu$m and $err_2 = 0.25\ \mu$m.

So we conclude that the micropipes with large diameters of their cross-section areas can be quantitatively estimated with better accuracy, especially when they are measured at small object-to-detector distance z_d. The value $\chi^2_{\min}$ is not important because it is determined by signal-to noise ratio. More important a sensitivity of the theoretical curves to the parameters D and D_0 which leads to better increasing χ^2 near the minimum point.

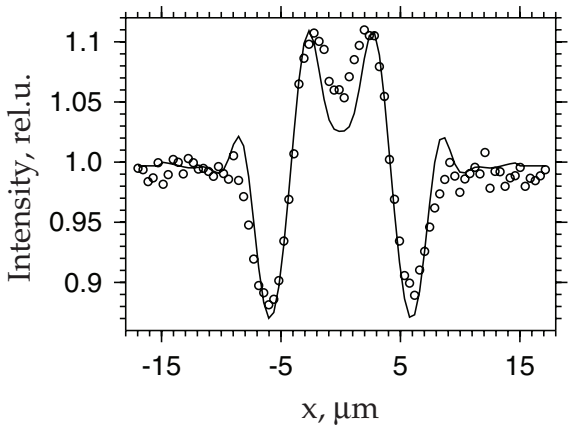

FIG. 7. Experimental data and simulated theoretical profile in the case of best coincidence for the second case. By fitting many profiles for various diameters of micropipe cross section we determined the diameters from the condition of best coincidence.

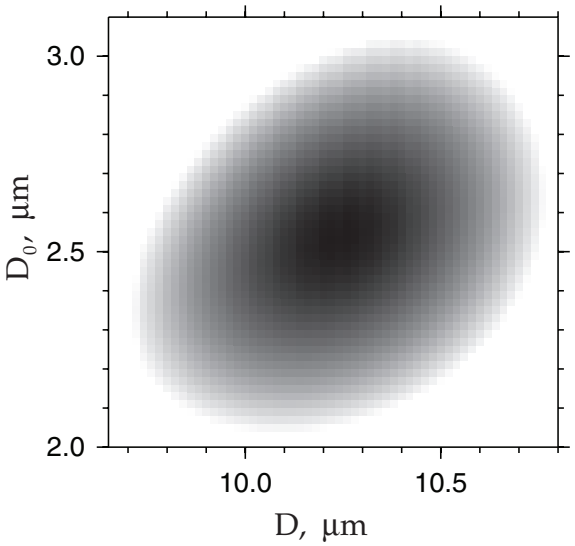

FIG. 8. A map showing the least square sum χ^2 as a function of D and D_0 in the second case. See text for details.

Though small values of z_d are preferential, however, at such distances, undesirable scattering can be sometimes registered, which leads to extra noise of the experimental data. As a result, it is impossible to obtain an accurate fitting of the experimental data. On the other hand, micropipes with large cross section areas may have more complicated shapes different from the assumed elliptical ones. As for micropipes of small cross section, there is a problem in obtaining both diameters with a good accuracy. One of solutions may be the use of monochromatic SR beam, instead of pink one, which is, however, not so simple owing to drastic loss of the intensity.

VI. SUMMARY

In-line SR phase-contrast technique is now well-established for imaging micro structure in materials, soft condensed matter, biological objects, etc. A wide variety of features is investigated when one fully exploits the coherence, the brilliance and the resolution provided by the modern SR sources. However, at quite many synchrotron facilities, the increase of brilliance can be achieved

by virtue of limited time coherence. Polychromatic SR beam still provides important qualitative, or semiquantitative, pictures of different objects.

We have demonstrated that, since the theory of phase contrast is well established, image simulation is a powerful means of quantitative characterization on a micro-scale. The cross-sections of micropipes in industrial size of SiC crystals are determined by using the computer program. Simulating procedure is described in detail. The peculiarities of computer simulation are analyzed and the experimental examples are provided. We have considered the general problems in estimating the accuracy of parameters from the least square fitting procedure.

ACKNOWLEDGMENTS

The experimental part was supported by the Creative Research Initiatives (Functional X-ray Imaging) of MEST/KOSEF of Korea. The work of VGK was partially supported by RFBR grant N. 13-02-00469, by The Ministry of education and science of Russian Federation, project 8364.

[1] J. Heindl, W. Dorsch, H. P. Strunk, St. G. Müller, R. Eckstein, D. Hofmann, and A. Winnacker, Phys. Rev. Lett. **80**, 740 (1998).
[2] X. R. Huang, M. Dudley, W. M. Vetter, W. Huang, S. Wang, and C. H. Carter, Jr., Appl. Phys. Lett. **74**, 353 (1999).
[3] S. Milita, R. Madar, J. Baruchel, M. Anikin, and T. Argunova, Mater. Sci. Eng. B **61-62**, 63 (1999).
[4] T. S. Argunova, M. Yu. Gutkin, J. H. Je, V. G. Kohn, and E. N. Mokhov, *Physics and Technology of Silicon Carbide Devices* (Intech Publications, Croatia, 2012), Section 1, Chapter 2, 27.
[5] J. Härtwig, J. Baruchel, H. Kuhn, X-R. Huang, M. Dudley, and E. Pernot, Nucl. Instrum. Meth. B **200**, 323 (2003).
[6] D. Nakamura, S. Yamaguchi, Y. Hirose, T. Tani, K. Takatori, K. Kajiwara, and T. Kimoto, J. Appl. Phys. **103**, 013510 (2008).
[7] V. G. Kohn, T. S. Argunova, and J. H. Je, Appl. Phys. Lett. **91**, 171901 (2007).
[8] M. Yu. Gutkin, A. G. Sheinerman, M. A. Smirnov, V. G. Kohn, T. S. Argunova, J. H. Je, and J. W. Jung, Appl. Phys. Lett. **93**, 151905 (2008).
[9] T. S. Argunova, V. G. Kohn, J. W. Jung, and J. H. Je, Phys. Stat. Solidi (a) **206**, 1833 (2009).
[10] V. G. Kohn, T. S. Argunova, and J. H. Je, J. Phys. D: Appl. Phys. **43**, 442002 (2010).
[11] A. M. Afanasev and V. G. Kohn, Sov. Phys. Crystallogr. **22**, 355 (1977).
[12] A. Snigirev, I. Snigireva, V. Kohn, S. Kuznetsov, and I. Schelokov, Rev. Sci. Instrum. **66**, 5486 (1995).
[13] T. S. Argunova, V. G. Kohn, and J. H. Je, J. Surface Investig. X-ray, Synchr., Neutron Techn. **2**, 861 (2008).
[14] V. G. Kohn, T. S. Argunova, and J. H. Je, J. Surface Investig. X-ray, Synchr., Neutron Techn. **6**, 840 (2012).